ACS APPLIED MATERIALS & INTERFACES

Research Article

www.acsami.org

Microscopy Study of Structural Evolution in Epitaxial $LiCoO_2$ Positive Electrode Films during Electrochemical Cycling

Haiyan Tan,*[,†,‡] Saya Takeuchi,[‡] K. Kamala Bharathi,[‡,§] Ichiro Takeuchi,[§] and Leonid A. Bendersky*[,‡]

[†]Theiss Research, La Jolla, California 92037, United States

[‡]Material Measurement Laboratory, National Institute of Standards and Technology (NIST), Gaithersburg, Maryland 20899, United States

[§]Department of Materials Science and Engineering, University of Maryland, College Park, Maryland 20742, United States

Supporting Information

ABSTRACT: The evolution of interface between the epitaxial thin film $LiCoO_2$ (LCO) electrode and liquid electrolyte and inside the LCO film during electrochemical cycling has been analyzed by high resolution scanning transmission electron microscopy. Relaxation of sharp translational domain boundaries with mismatched layers of CoO_2 octahedra occurs during cycling and results in formation of continuous CoO_2 layers across the boundaries. The original trigonal layered structure of $LiCoO_2$ tends to change into a spinel structure at the electrode/electrolyte interface after significant extraction of Li from LCO. This change is more pronounced at 4.2 V peak of CV, indicating lower stability of the layered LCO structure near its surface after Li is extracted above 60%. The transformed structure is identified to be close to Co_3O_4, with Co both on tetrahedral and octahedral sites, rather than to $LiCo_2O_4$ as it was suggested in earlier publications. Electron energy-loss spectroscopy measurements also show that Co ions oxidation state is reduced to mixed valence state Co^{2+}/Co^{3+} during the structure changes to spinel rather than oxidized.

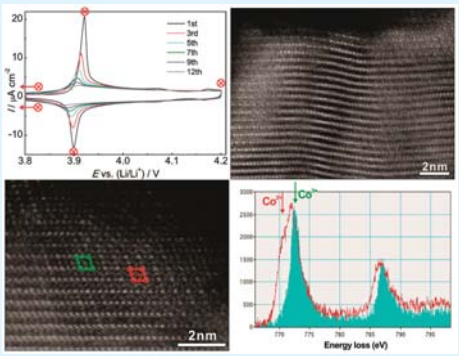

KEYWORDS: *structural evolution, $LiCoO_2$, epitaxial thin films, electrochemical cycling, STEM*

INTRODUCTION

Lithium-ion batteries (LIBs) are widely used in variety of mobile devices (cellular phones, personal computer, and digital cameras) and recently in hybrid and fully electric (e.g., Tesla, Chevrolet Volt) vehicles. LIBs have great success in being an essential part in different technologies; however, because of the batteries' flammable liquid electrolytes, there are still issues of safety and longevity/reliability in severe operating conditions. A promising solution is replacing the flammable liquid electrolyte with inorganic Li-ion conducting solids, thus switching to all-solid-state LIBs.[1,2] One type of such batteries is a multilayer stack comprising a positive electrode, an electrolyte, and a negative electrode, all in solid state thin-film form; the solid−solid interfaces between electrodes and electrolyte, as well as microstructure inside each component, are expected to strongly affect the battery performance.[3] Despite clear technological importance of the all-solid-state LIBs, there are only limited studies focused on the issues of internal interfaces in these batteries.[4−6] Although this paper deals with processes occurring in positive electrode/liquid electrolyte interfaces, studying growth and electrochemistry of a thin film positive electrode is a part of our broader study of all-solid-state thin film-based batteries.

Thin-film metal oxides have been demonstrated for myriad applications including electrode for LIB,[7,8] UV photodetectors,[9,10] and gas sensors.[11] Among them, $LiCoO_2$ (LCO) material has been extensively studied as a positive electrode for LIBs, but its local structure change during or after electrochemical cycles, especially at the electrode/electrolyte interfaces, is still not fully understood.[12] Advanced transmission electron microscopy (TEM) is capable of providing the most informative insight into crystal structure and defects, chemical composition, and the electronic states of transition metals on atomic scale,[13−17] the insight essential for understanding the electrode/electrolyte interface behaviors. Most of the TEM studies on the LCO materials were on positive electrodes prepared by mixing LCO powders with the carbon black conductor and binders.[18,19] For TEM observations of different stages of electrochemical cycling, the electrodes were disassembled, washed out, separated from the binder and conductor, and then LCO powder was crashed and collected on a TEM grid for studies.[20] This procedure contributes uncertainties on what the studied particle's surface represents, either the one that was in direct interaction with electrolyte, or the one in contact with other components of constituted a positive electrode. For example, the cathode material particles

Received: December 9, 2015
Accepted: February 25, 2016
Published: February 25, 2016

ACS Publications © 2016 American Chemical Society

DOI: 10.1021/acsami.5b12025
ACS Appl. Mater. Interfaces 2016, 8, 6727−6735

studied by Wang et al.[21] were found to be altered inhomogeneously, but the distribution of those particles was lost during the TEM sample preparation process, and no direct evidence could be provided to illustrate why some particles were altered significantly more than others.

To investigate binder/conductor-free positive electrode for the structural changes (especially at the interfaces) during cycling, it was proposed to investigate positive electrodes in a form of epitaxial films.[7,8] Epitaxial growth of LCO films on $SrTiO_3$ (STO) substrates of different orientations by Pulsed Laser Deposition (PLD) will expose various crystallographic orientations; the approach has drawn significant attention recently, mostly for the film-based all-solid Li-ion batteries.[22,23] In our recent work, we studied LCO films PLD deposited on $SrRuO_3/SrTiO_3$ (SRO/STO) substrates of different STO orientations (films of perovskite SRO grown on perovskite STO substrates are in cube-on-cube orientations); the work has demonstrated that using SRO enables successful electrochemical testing and supports epitaxial deposition.[24] The epitaxial growth nicely controls the crystal orientation of the anisotropic trigonal LCO films, thus controling a Li-ion migration path. In previous work, we demonstrated that charge transfer resistance could be strongly influenced by the orientation and growth mode of LCO thin films.[24]

The focus of this work is on investigation of structural changes occurring at different stages of charge/discharge process for the LCO films deposited on (111) STO. Although LCO has been studied extensively, it was selected for this work as a model system for better understanding the possible advantages of using epitaxial thin films as binder/conductor-free electrodes, with intention further to apply the approach to studying advanced cathode materials. The TEM in this work demonstrates the dependence of structural surface evolution at different stages of cycling as well as the role of crystallographic orientation of different facets. Additional study of the films deposited on the (100) STO substrate (results presented in the Supporting Information) supports the major observations. By experimenting with the LCO cathode, we also demonstrate that the epitaxial thin films can be useful to observe and study crystallographic interfaces between the single crystal-like positive electrode and liquid electrolyte at different stages of electrochemical cycling by high-resolution TEM. The approach overcomes certain ambiguities that present in studying positive electrodes made from powders mixed with binders and conductors. We believe that the same approach can be useful in understanding structural changes occurring in advanced Li-ion and Na-ion positive electrode materials.

EXPERIMENTAL SECTION

SRO (electrical conductive layer) and LCO thin films were deposited sequentially on STO (111) substrates (square shape, approximately 0.5 cm × 0.5 cm) using PLD. SRO was deposited at 650 °C and LCO deposited at 600 °C temperature of the substrate, 27 Pa oxygen pressure, and a KrF laser (wavelength 248 nm). Extra lithium containing $Li_{1.4}CoO_2$ ceramic pellet from Toshima Co. (Certain commercial equipment, instruments, or materials are identified in this document. Such identification does not imply recommendation or endorsement by the National Institute of Standards and Technology, nor does it imply that the products identified are necessarily the best available for the purpose.) was employed for all the depositions. The laser repetition rate was 10 Hz, and the laser energy was 100 mJ per pulse. The STO substrates were cleaned with acetone and ethanol for 10 min each in a sonicator. All the substrates were thoroughly dried with nitrogen before they were introduced into the deposition chamber, which was initially evacuated to a base pressure of ~5×10^{-4} Pa. LCO and SRO targets (2.54 cm diameter) were placed on a target holder, which is placed at a distance of 6.8 cm from the substrate. Before each deposition, the targets were presputtered for 5 min to eliminate the impurities on the surface.

Cyclic voltammetry (CV) was carried out with a three-electrode cell, in which Li metal served as counter and reference electrodes. Working electrode LCO/SRO/STO area was determined by Viton O-ring, which was 0.13 cm^2. Electric contact between current collector and the sample was obtained with Ag paste or carbon paste. Electrolyte was 1 mol dm^{-3} $LiClO_4$/propylene carbonate (PC) (BASF, battery grade), and the sweep rate was 0.1 mV/s. The commercially popular $LiPF_6$ electrolyte is avoided here due to its potential chemical reaction with LCO.[25−27] Our experiments also show that the capacity decrease with $LiPF_6$ as electrolyte is much faster than that with $LiClO_4$ (Figure S6). Electrochemical measurement was carried out with BioLogic VSP-300 in an Ar-filled glovebox set for 30 °C. All the potentials refer to Li/Li^+. To verify that the sweep rate is slow enough for LCO film to reach equilibrium state at each extraction voltage, the half-cells were disassembled when extraction voltages reached 3.94 V either immediately or held for 8, 100, or 140 h. TEM results do not show obvious difference for those samples (Figure S1), which testifies that the selected sweep rate is slow enough for homogeneous Li extractions from the LCO film. Thus, most cells were disassembled immediately after electrochemical experiments for the TEM study; all the samples were washed with dimethyl carbonate (BASF, battery grade) and sealed in an Ar atmosphere for a protection during sample transfer.

Electron-transparent cross-sectional TEM lamellae were prepared by a focus ion beam (FEI Nova 600 NanoLab). Carbon and Pt were coated on the LCO film surface in advance to protect it against ion damage. The lamellae were milled and cleaned by Ga ions to typically 50 nm in thickness for good electron transparency. High angle annular dark field-scanning transmission electron microscopy (HAADF-STEM) investigation was performed on the prepared lamellae using a probe-corrected FEI Titan 80−300 microscope operating at 300 kV. The probe is typically corrected to provide a spatial resolution of 0.1 nm. The probe convergence angle is 24 mrad, and the HAADF inner and outer collection angles are 70 and 400 mrad, respectively. Electron energy-loss spectroscopy (EELS) spectrum was acquired in STEM mode by GIF Tridium with quasi-simultaneous acquisition of low-loss and Ti-L core-loss edge for its precise peak position. A 0.05 eV/channel dispersion was applied, which provided an energy resolution of 0.7 eV by full-width of half-maximum (fwhm) of a zero loss peak.

RESULTS AND DISCUSSION

Figure 1 shows cyclic voltammograms (up to 12 cycles) measured for the LCO/SRO/STO (111) film. Broad and low oxidation peak around 3.8 V is attributed to the oxidation of electrolyte.[28] In the first cycle, the largest redox couple is observed around 3.90 V, and two small redox couples are observed around 4.05 and 4.15 V; according to the literature, these peaks are attributed to phase transformations typical for the layered LCO.[19] The initial appearance of 4.05 and 4.15 V peaks indicates that the film was initially structurally uniform; however, these peaks are not observed clearly in the later cycles, which can be interpreted as less clear phase transitions between the trigonal $LiCoO_2$ and monoclinic Li_xCoO_2 (x = 0.5) phases.[19] As the cycle number increases, redox peaks at the 3.90 V redox peaks also become lower and wider after a few cycles, which can also be interpreted as less clear phase transitions. The similar electrochemical behavior was also observed for the LCO/SRO/STO (100) (Figure S2a). Note that according to TEM, the LCO/SRO interface after 12 cycles remained intact, thus the broadening and shift of peaks are not due to the changes in electric contact at LCO/SRO interface and should be attributed entirely to the changes occurring in the LCO film.

DOI: 10.1021/acsami.5b12025
ACS Appl. Mater. Interfaces 2016, 8, 6727−6735

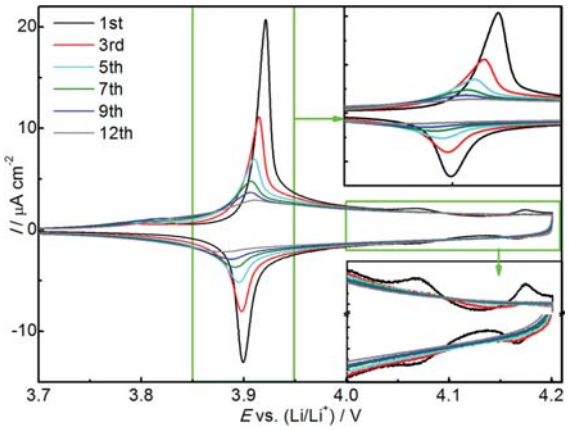

Figure 1. Cyclic voltammograms of LCO/SRO/STO (111) for different number of cycles. Note that with increasing number of cycles, the peaks become less prominent, and the approximately 3.9 V peak systematically moves to lower voltage.

Cathodic capacity decreases gradually as cycle number increases; after 12 cycles, it is 18% less than for the first cycle. A couple of possible explanations for the observed decrease in cathodic capacity could be offered: (1) the buildup of a surface film at the electrolyte/LCO interface from oxidation of electrolyte;[28] (2) spinel phase formation at a surface of LCO,[20,29] which loses its capacity and restricts the Li ion movement from the interior of the LCO film.[29] The hypothesis of the spinel formation at the surface is also supported by the increase of Li^+ transfer resistance at 4.2 V as a cycle number increases, as measured by impedance spectroscopy (Figure S3). Along with the increase of over potential after first five cycles, these measurements indicate the modifications of a crystal structure of the LCO film. It is interesting to note that the peaks' decay can be restored to a certain extent by annealing the samples at 550 °C in air (Figure S2b). This observation suggests that the structure modification induced by cycling and discussed below can be restored to the original trigonal LCO structure.

Note that the capacity decrease is faster than that for commercial batteries. One of the reasons is due to the fact that the commercial batteries are built of composite electrodes (mixture of active material with carbon and polymers as binder);[30] in our system, single-crystal-like epitaxial thin films are employed. Delithiation/lithiation reaction of LCO comes along with the lattice expansion/shrinking,[31] and in the case of composite electrodes, polymers serve to keep an LCO electrode intact even after developing crack due to the lattice deformation.[21] Our binder free, thin films cannot recover once the cracks form, which makes these electrodes vulnerable to physical stress during CV, and accordingly the cycle ability of the epitaxial LCO is not good compared to commercialized batteries. However, it is of minor importance considering that the major goal of our study is observing detailed structural evolution.

A cross-section of a pristine sample in Figure 2, panel a shows that the film has almost uniform thickness, but its top surface has facets; overall, the top surface consists of (001) and {104} crystallographic facets of the trigonal layered LCO. The horizontal surface is the (001) plane dictated by the growth direction and orientation relationship, whereas the inclined facets are the {104} lowest energy surfaces.[32,24] A high-resolution image of the LCO/SRO interface in Figure 2, panel b indicates that the LCO grows epitaxially on top of SRO without defects, and the SRO conductive layer perfectly transfers the crystal orientation of the STO substrate to the LCO layer. HAADF-STEM image of LCO shows only columns of high-Z (namely Co ions in this case),[33,34] which fit perfectly to the expected trigonal layered LCO. The model shown in Figure 2, panel c demonstrated how the LCO layer grows on SRO by maintaining the -ABC- oxygen ions sequence at the interface. The LCO (001) plane is parallel to the film surface by the nature of epitaxial growth on SRO (111). Since it has been previously demonstrated that Li ions during electrochemical cycling diffuse much more efficient along the 001 planes,[35,24] for this film configuration, the Li ions' transfer from the electrode to electrolyte is expected mostly through the {104} planes rather than across the (001) plane.

Although the entire LCO film adopted the same orientation of LCO (001)//SRO (111) from the STO substrate, by the nature of island growth and not perfect atomic flatness of a SRO surface, the film consists of rotational (60° rotation around $[001]_{LCO}$) and translational domains shifted in $[001]_{LCO}$ by one or more atomic planes. Boundaries between such translational domains are observed in Figure 3, panel a as

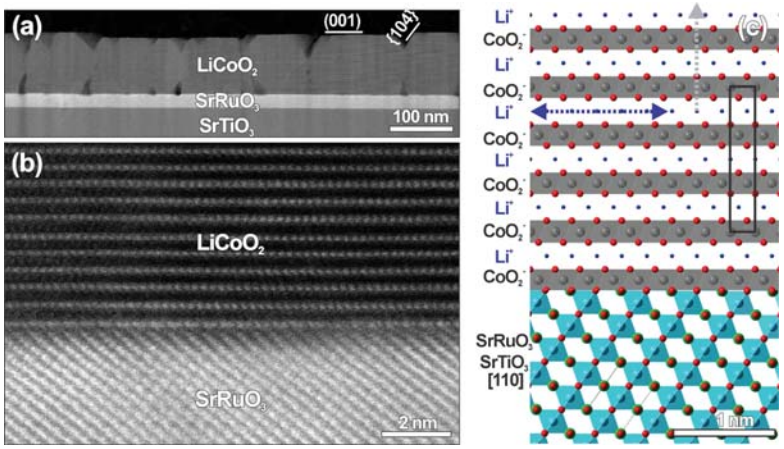

Figure 2. (a) HAADF-STEM overview showing epitaxial LCO film with growth facets. (b) The atomic resolved STEM image at the LCO/SRO interface supporting epitaxial relationship. (c) Structure model of the LCO/SRO interfaces.

DOI: 10.1021/acsami.5b12025
ACS Appl. Mater. Interfaces 2016, 8, 6727−6735

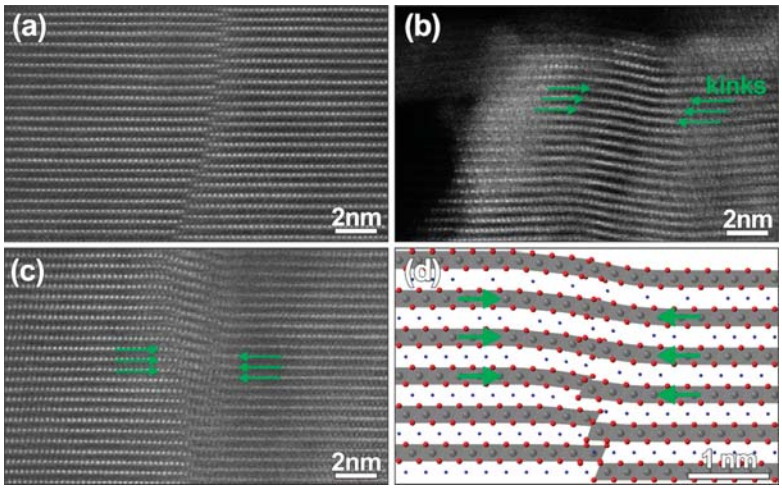

Figure 3. (a) Sharp domain boundary of the pristine sample. (b) Twisted Co plane on the film surface after electrochemical cycles. (c) The plane is severely twisted on the surface of the film, but the central part remains intact. (d) A crystal model illustrates the twisted plane structure.

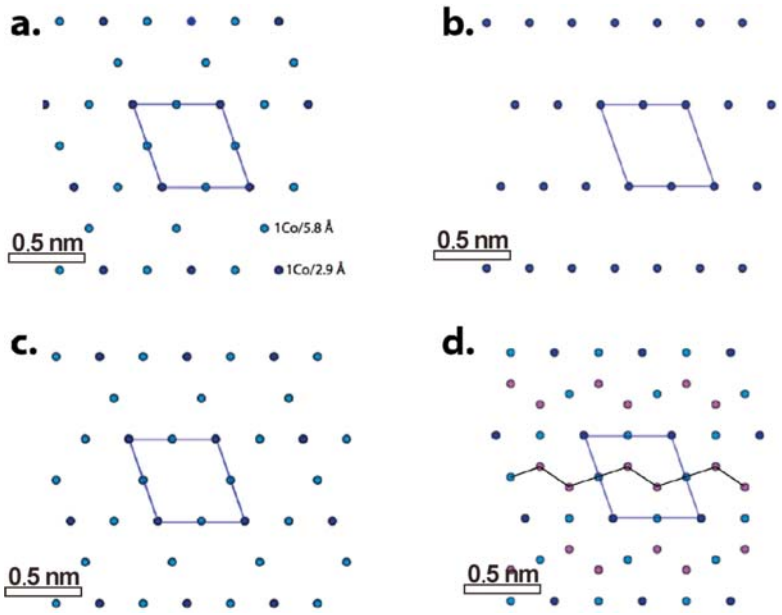

Figure 4. Projection of Co columns for (a) LT-LCO spinel in [1−10] direction; (b) layered trigonal HT-LCO in [010]; (c) $Li_{0.5}CoO_2$ spinel in [1−10]; (d) Co_3O_4 binary spinel in [1−10].

sharp and flat. In Figure 3, panel a, Co planes in the left domain are a continuation of Li planes in the right domain; however, the oxygen sublattice is common for both domains. Significant changes to the translational domains occur after a full electrochemical cycle: the sharp domain interfaces are less frequently observed and instead the translation domain boundaries show deviation of the Co planes from initial $(001)_{LCO}$, as shown in Figure 3, panel b. Those kinks provide gradual continuation of the Co planes between the shifted domains. Those bent planes are more often seen close to the film's surface, while inside the LCO film, sharp translational boundaries can still be observed (Figure 3c). The observation suggests that the translation domains boundaries were altered during the electrochemical experiment and from the changes initiated from the film's surface contacting the electrolyte. The translational boundaries, by the presence of domains defects/vacancies, most probably provide sufficient diffusivity of Li to move across the films. Thus, Li ions can be extracted along those domain boundaries and leave a large amount of Li vacancies behind along the boundary.[36] The oxygen sublattice will also slightly expand due to less Coulomb force attraction. Apparently this process creates conditions to minimize the interfacial energy by forming continuity of the Co plane; thus, adjustment of O and Co positions occurring near the boundary forms the observed kinks and inclined twists between the domains, as shown in Figure 3, panel d. Overall, continuous cycling is contributing to higher density of the kinks. This is supported by the increased diffusion coefficient at single-grain boundaries or defect regions as observed by atomic force microscopy[36] as well as by theoretical calculation.[5]

During electrochemical cycling of the films, the charging/discharging was stopped at the voltages of characteristic redox peaks of the cyclic voltammogram (Figure 1). Then the films were removed from the electrolyte and carefully washed; a

DOI: 10.1021/acsami.5b12025
ACS Appl. Mater. Interfaces 2016, 8, 6727−6735

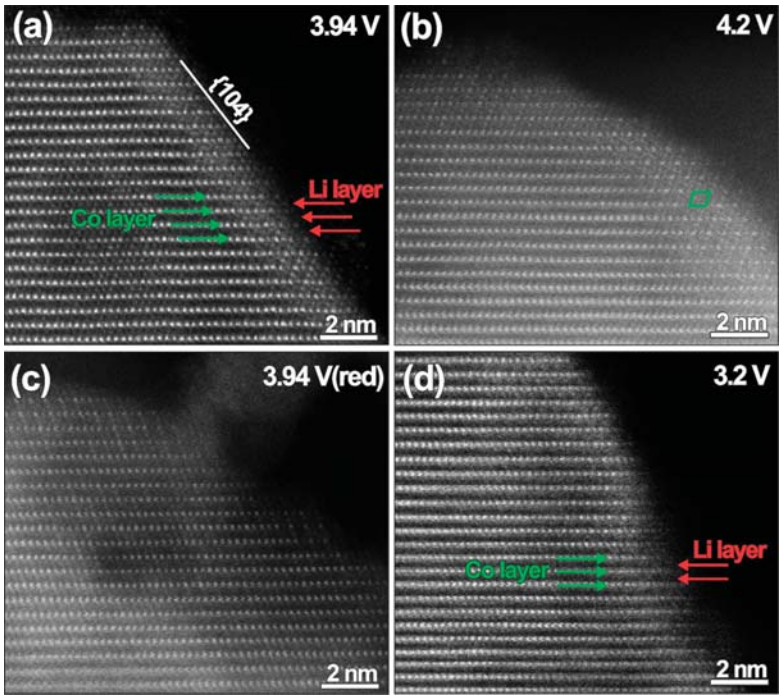

Figure 5. (a) The atomic resolved HAADF-STEM images at (a) 3.94 V, (b) 4.2 V, (c) 3.94 V (reduction), and (d) 3.2 V. The images show the cation rearrangement mainly at the film surface.

TEM lamella was extracted from the samples by FIB. HAADF-STEM shows that the studied films at different stages of charging have the structure in its majority similar, which is indicating that the LCO crystal structure is preserved during the cycles. However, the pronounced feature was the observation of structural changes near the film's surface contacting electrolyte directly. Since the features suggest spinel structures, we will first consider the known spinel LCO structures and their structural projections relevant to the analysis of TEM images presented below.

The spinel structure was first reported for LT-LCO, the $LiCoO_2$ phase synthesized at lower (<400 C) temperatures.[37−39] The structure, called "quasi-spinel" in ref 38, has $Fd\bar{3}m$ space group of spinel, however different from known spinel in its stoichiometry and presence of Co or Li at their tetrahedral sites. Figure 4, panel a shows projection of the LT-LCO structure in [1−10] cubic direction; it is compared with the trigonal $R\bar{3}m$ layered high-temperature HT-LCO, Figure 4, panel b. In these structural projections, only columns of Co ions are shown, which is relevant for the analysis of HAADF-STEM images that are sensitive to high-Z columns of atoms; the circles representing columns have two colors according to the density of Co along the projection: darker for higher density, 1 Co/2.9 Å, and lighter for twice lower density, 1 Co/5.8 Å. Brightness of the spots visible in HAADF-STEM images and representing atomic columns will be according to these densities. Thus, for the LT-LCO, the strong spots form a rhombus, as shown in Figure 4, panel a, with the weaker spots in the middle of the rhombus sides, whereas for the trigonal HT-LCO, all spots are of equal intensity and position along a similar rhombus, as shown in Figure 4, panel b. In Figure 4, panel c, a projection of the delithiated $Li_{0.5}CoO_2$ is shown; the projection is the same as for the LT-LCO, although the structures differ. For the LT-LCO, both Co and Li are in octahedral positions, with alternating 2CoLi and Co2Li ordered layers, whereas for $Li_{0.5}CoO_2$, Li is in tetrahedral A positions of AB_2O_4 spinel. Figure 4, panel d shows a projection of the binary spinel Co_3O_4; in this structure, one Co is in tetrahedral sites. Because of the tetrahedral sites, in addition to the arrangement of rhombus similar to other LCO spinel structures, there is the presence of columns inside the rhombus that form a zigzag appearance. Note that all three spinel structures, LT-LCO, $Li_{0.5}CoO_2$, and Co_3O_4, will yield similar electron diffractions; thus, it is difficult to differentiate between the phases without structural imaging.

Figure 5, panel a shows TEM results for the sample stopped at 3.94 V (see Figure 1), just after the prominent peak (fast Li extraction) was reached. Assuming uniform Li extraction from the LCO film, this stage corresponds to ∼20% of Li extraction. The HAADF-STEM image shows arrangement of Co columns inside the LCO film according to the trigonal LCO structure in [010] zone axis (see Figure 4b); the rows of bright spots are layers of Co, and space between the layers corresponds to Li layers (invisible). According to the literature,[31] the LCO at this stage of Li extraction changes to a monoclinic structure; projection of Co for the monoclinic structure has almost the same arrangement as the triclinic LCO. Near the film's surface, especially at the LCO {104} facets, bright spots located within the Li layers are visible; since Li is not visible in the used imaging condition, the observation suggests presence of Co ions that occupy Li vacancies formed during Li extraction during the cycling. Such presence of Li/Co in the Li layers is mainly observed for the {104} facets due to the fact that these facets have open channels for Li extraction. Such presence of transition metal cations in Li layers near a surface was also previously observed in the cycled $Li_{1.2}Ni_{0.2}Mn_{0.6}O_2$.[40,41]

Figure 5, panel b shows the sample stopped at 4.2 V during its discharge; according to CV, approximately 60% of Li have been extracted at this stage. It is already an extreme condition close to loss of stability of the layered LCO structure.[42,43] Near

DOI: 10.1021/acsami.5b12025
ACS Appl. Mater. Interfaces 2016, 8, 6727−6735

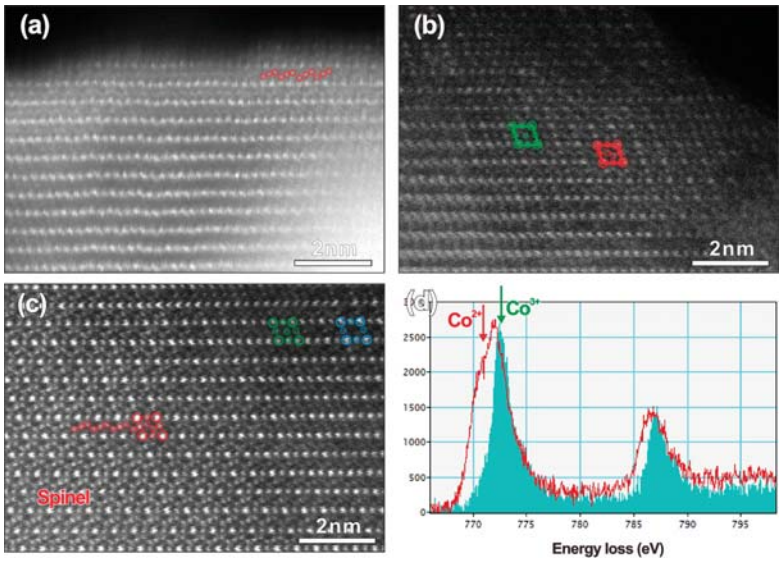

Figure 6. Different stages of the structure changes from the initial layer structure to the spinel structure from the sample stopped at 4.2 V in a cycle. (a) The initial state showing the rearrangement of tetrahedral site. (b) Later stage shows the rhombus pattern. (c) The final state of a perfect spinel structure on the left side, while the right site is still layered structure. (d) Core-loss EELS on the Co-$L_{2,3}$ edge shows that the Co ions in the spinel structure have its oxidation state lower than original 3+ in the layer structure (red, spectrum from the transformed spinel region; blue, spectrum from the intact triclinic LCO area).

the film's surface, especially for the {104} facets, the intensity contrast is noticeably different from the film's interior; it is very clear that Co ions are also present in the Li layer. The Co-related strong spots form a rhombus pattern (indicated as a green rhombus in Figure 5b), with weaker spots in the middle of rhombus sides. The observed arrangement of spots suggests long-range order structure, thus the local phase transition to a new phase. The observed positions of spots and their intensities would fit either LT- $LiCoO_2$ or $Li_{0.5}CoO_2$ spinel structures, as [1−10] projections in Figure 4, panels a and c, respectively, suggest. Considering the 60% extraction of Li at that state, the observed distribution of intensities would rather correspond to the spinel $Li_{0.5}CoO_2$ with Li (not visible) in tetrahedral positions. Figure 5, panel c shows the sample stopped at 3.94 V but during the reduction (lithiation) part of the cycling. The rhombus arrangements can be seen only occasionally in some areas, certainly not as pronounced as at 4.2 V in Figure 5, panel b. The structure is predominantly trigonal (Figure 4b) with only minor presence of the spinel-like order. This structural observation supports the reversibility of the charge/discharge process measured by electrochemistry; it is expected that at the same potential the structural state of the samples should be the same or similar for close to the equilibrium slow rate cycling. Figure 5, panel d shows an image of the sample that was brought back to the open circuit voltage at 3.2 V. The image shows the film has entirely the trigonal layered phase, same as in its initial condition. Only near the film's surface (approximately 1 nm from the surface), the presence of weak bright spots in the Li layer (indicated by red arrows in the figure) suggests the remnant presence of Co partially substituting Li. Nevertheless, overall the Co cations moved back to its original positions in the Co layer after a cycle was completed.

Figure 6 shows images that help us to understand in more detail the structural changes occurring at 4.2 V stage. Figure 6, panel a shows a 1 nm thick (001) surface layer, where some bright spots can be seen within the Li layers, which indicate the presence of some Co atoms in the Li layers. A closer look shows that these Co atoms do not line up but rather form a zigzag alignment (indicated by red cycles). This observation suggests that those Co atoms are actually occupying not octahedral Li positions of the trigonal phase but rather at tetrahedral sites characteristic for a spinel structure (more clear in Figure 6c). Also note that the structural pattern along the (001) plane is still not established, which indicates that this is an early stage of the structural change. Figure 6, panel b shows an established pattern of rhombuses near the film's {104} surface. In some regions (indicated by a green rhombus), the rhombus pattern has distribution of intensities and position of spots that correspond to the spinel $Li_{0.5}CoO_2$ structure (Figure 4b). However, in the areas close to the surface, the rhombus patterns have two bright spots inside (see red rhombus, corresponding to Figure 4d), which clearly indicate variations in a local structure. The prominent structural change is clearly seen in the region shown in Figure 6, panel c. On the left part of the image, the whole region has been interpreted as having a spinel Co_3O_4 structure, whereas the right side the crystal remains in its original layered structure. Positions of zigzagging spots within the Li layer and alternation of intensity of spots in Co layer correspond well to the positions of Co columns in [1−10]-oriented Co_3O_4 (or more conservatively (Co,Li)-Co_2O_4) as shown in Figure 4, panel d. The crystal planes between the regions of spinel and layered structure are continuous, thus suggesting the common for both structures an oxygen ccp-like sublattice; thus, the structural changes occur gradually by chemical reordering of Co on the same oxygen framework and cause minimum strain.

Significant structural transformations were observed on the LCO/SRO/STO(100) samples after being charge−discharged over 30 cycles (Figure S4). The 10 nm thick surface layer of LCO has mostly transformed to the spinel structure identifiable by rhombus patterns (Figure S4b). Furthermore, there are two types of rhombus patterns, which differ by the presence of bright spots inside the rhombuses (Figure S4c): (1) at a few

DOI: 10.1021/acsami.5b12025
ACS Appl. Mater. Interfaces 2016, 8, 6727−6735

atomic layers from the film's surface, the rhombus pattern does not have the bright spots inside (marked as a blue rhombus with circles); (2) a few nanometers below the surface, each rhombus pattern (red rhombus) has two bright spots inside. This observation suggests that light Li atoms or no atom present at the tetrahedral sites at the film surface but at the areas below the surface Co atoms do considerably occupy the tetrahedral sites.

The structural change during cycling from the trigonal LCO to the spinel has been suggested previously based on electron diffraction; however, high-resolution imaging and structural details were missing.[20,21] Our finding is in agreement with the observations that "the structure changes first at the surface of crystals but eventually extends throughout some crystals".[20] Gabrisch et al. have interpreted their diffraction results (lattice parameter and symmetry) as fitting well to the delithiated spinel $Li_{1+y}Co_2O_4$ with Li at the tetrahedral positions.[20] On the basis of electron diffraction and modeling, Wang et al. also suggested that the spinel has its tetrahedral sites occupied by Li.[21] However, our high-resolution STEM imaging results offer a new insight into structural details of the transformed spinel structures that were not available from the cited above electron diffraction studies. We have directly imaged two types of spinel structures: (1) one type without Co on tetrahedral sites (blue rhombus in Figure S4c) having spinel $Li_xCo_2O_4$ with Li at the tetrahedral site; and (2) another type with Co on the tetrahedral sites (red rhombus) that matches either spinel Co_3O_4 or $(Li,Co)Co_2O_4$ structures, which is also observed in the samples stopped at 4.2 V during charge/discharge cycles (Figure 6).

This imaging-based supposition is also strongly supported by EELS measurements from the areas that have structural images of spinel, which is able to identify oxidation state of transition metals.[15,44] The Co-$L_{2,3}$ core-loss edge from those spinel areas (marked by red rhombus) shows a lower onset than that from the areas of the layered structure, indicating that the oxidation state of Co is lower than 3+ of delithiated $LiCoO_2$ (Figure 6d). It also rules out the possibility of $LiCo_2O_4$ structure, which has 3.5+ for Co in octahedral B-position in the area. This indicates that Co in A-site is in fact reduced to 2+ during formation of the spinel rather than oxidized.[44,17] Previously, Takamatsu et al. studied the surface of the $LiCoO_2$ electrode that is in contact with organic electrolyte solutions and its bulk embedded inside the electrode by XPS. They revealed that the surface went through a completely different reaction process than the bulk. The surface was irreversibly reduced to Co^{2+}/Co^{3+}, but the bulk was reversibly oxidized to Co^{4+} in the charge/discharge process. They proposed a hypothesis that the surfaces form Co_3O_4 or other species during charging and subsequently cannot be reduced during discharging.[43] Here, we directly observed the significant presence of Co_3O_4-like phase concentrated on the LCO film surfaces, which strongly supports this hypothesis. The Co reduction occurring at the surface of LCO electrode can be the initial deterioration of LIBs that gradually propagates inside the LCO films with cycling and leads to capacity losses of the battery. In support of our observations, the defective spinel structure was also observed on surfaces of $Li_{1.2}Ni_{0.2}Mn_{0.6}O_2$ particles by Carroll et al.[40] Also, Qian et al.[45] have demonstrated significant changes in a shape of oxygen K edge from areas with transformed spinel structure, which indicates dramatic bonding changes between oxygen and cations leading to oxidation state change. It agrees with our observation of oxidation state changes of Co in the spinel structure. We need to emphasize that this cation movement and structure change are not due to the electron beam damage since STEM mode with low beam current was applied to minimize the radiation damage.[46] The beam was aligned in the substrate area and then shifted to the fresh area of interest. Typically, several images were acquired from those fresh areas and show no structural evolution during STEM image acquisition.

On the basis of our TEM studies, the capacity losses and changes in CV peaks height and width during iterative charge/discharge cycling of the studied epitaxial LCO films may be explained by the observed local structural changes:

(1) *Modification of translational domain boundaries.* After CV between OCV and 4.2 V, kinks were formed to continuously transfer the CoO_2 layers from one domain to another (Figure 3). In our previous paper, we reported that Li transfer between electrode/electrolyte takes place predominately at {104} facet,[24] whereas (001) planes have higher resistance to Li ion transfer. The continuous CoO_2 layers, which are parallel to the electrode/electrolyte interfaces, significantly hinder Li transition between electrode and electrolyte. Consequently, increase in Li ion transfer resistance at the electrode/electrolyte interface makes the oxidation/reduction of LCO much harder. This might also leave some region far below the surface layer bottom not reacted, resulting to inhomogeneity of reaction throughout the film. This inhomogeneous reaction may be one of the reasons for capacity decay we observed in CV.

(2) *Surface structural modification.* Trigonal to spinel structural transformation mainly occurs on the surface of the LCO electrode. The structure changes are initiated on the LCO film surface during CV (electrode/electrolyte interface) (Figures 5 and 6); and it is on the LCO surface where more than 50% of Li were extracted locally. In the formed spinel structure, both Li and Co atoms occupy the tetrahedral site (Figure S4). When the spinel structure change is minor (at 4.2 V in Figure 5b), it reverts to the trigonal LCO structure during lithiation and does not affect reversibility (Figure 5d). However, when the sample is cycled more and more times, and to higher voltage, a considerable amount of the electrode will convert into the spinel structure with Co at the tetrahedral site, especially at the film surface layer (Figure S4). It is well-known that Li_xCoO_2 is thermodynamically metastable and can cause heat and electrolyte combustion. The Li_xCoO_2 thermally decomposes with exothermic heat generation: $Li_{0.5}CoO_2 \rightarrow {}^1/_2LiCoO_2 + {}^1/_6\ Co_3O_4 + {}^1/_2O_2$ at 220 °C.[42] This exothermic reaction is likely to occur slowly at room temperature, especially when more than 50% of Li has been extracted locally. The excellent coherence between LCO and Co_3O_4 structure may also facilitate this structural change (Figure 6). The spinel surface layer eventually covers the electrode's surface and greatly hinders the Li ion transfer between electrode and electrolyte. This is expressed in much higher impedance and larger voltammetry peaks' separation for the films cycled more times (Figures S2 and S3). We believe that this mechanism is mainly responsible for the capacity loss in the studied LCO films.

DOI: 10.1021/acsami.5b12025
ACS Appl. Mater. Interfaces 2016, 8, 6727−6735

CONCLUSIONS

In this work, we demonstrate that epitaxial thin films can be used to model single crystal-like positive electrodes for observing by high-resolution TEM reactions on crystallographic cathode/electrolyte interfaces at different stages of electrochemical cycling.

(1) TEM observations showed that relaxation of translational domain boundaries with out-of-phase Co layers occurs during cycling; the relaxation results in the structural alignment, which makes the Co layers continuous across the boundaries. Such rearrangement reduces the energy of the translational domain boundary (makes it similar to the bulk energy) and possibly eliminates the movement/extraction of Li ions along these boundaries.

(2) Broadening and gradual lowering of the CV characteristic peaks were observed and interpreted as the effect of structural changes on cathodes' surfaces. For different stages of electrochemical cycling, 3.94 and 4.2 V during delithiation and 3.94 and 3.2 V during lithiation, HAADF-STEM shows that the original trigonal/monoclinic layered structure tends to change during delithiation into the spinel structure in the regions adjacent to the films' surfaces after significant extraction of Li (most pronounced for 4.2 V peak); during lithiation, restoration of the films to original trigonal layered LCO occurs. The observation indicates low stability of the layered LCO structure near its surface after Li is extracted above 60%.

(3) The transformation occurs by movement of Co into Li layers, first by occupying octahedral sites (the LT-LCO structure), and at higher Li extraction by forming a structure with Co in Li layers on tetrahedral sites; this structure is close to the Co_3O_4 spinel rather than to $LiCo_2O_4$, as it was suggested in earlier publications. EELS measurements of Co ions oxidation state suggest the presence of Co^{2+} in tetrahedral site in addition to Co^{3+} in octahedral sites in support of the structural observation.

(4) For the studied epitaxial thin film, prolonged cycling (up to 30 cycles) introduces severe damage in the form of structural damage to the LCO surface at the electrode/electrolyte interface.

ASSOCIATED CONTENT

Supporting Information

The Supporting Information is available free of charge on the ACS Publications website at DOI: 10.1021/acsami.5b12025.

HAADF-STEM images of the LCO films deposited on the STO(111) and STO(100) surfaces, which was studied at different cycling conditions; cyclic votammogram and the impedance spectroscopy of LCO/SRO/STO(100) (PDF)

AUTHOR INFORMATION

Corresponding Authors

*E-mail: Haiyan.tan1@gmail.com.

*E-mail: leonid.bendersky@nist.gov.

Notes

The authors declare no competing financial interest.

ACKNOWLEDGMENTS

Andrew A. Herzing and Babak Nikoobakht from NIST are greatly appreciated for their help in using instruments in their laboratories as well as for valuable discussions. H.T. acknowledges support from the U.S. Department of Commerce, National Institute of Standards and Technology under financial assistance Award Nos. 70NANB14H027 and 70NANB15H025. Official contribution of the National Institute of Standards and Technology; not subject to copyright in the United States.

REFERENCES

(1) Kim, J.; Eom, M.; Noh, S.; Shin, D. Performance Optimization of All-Solid-State Lithium Ion Batteries Using a Li_2S-P_2S_5 Solid Electrolyte and $LiCoO_2$ Cathode. *Electron. Mater. Lett.* **2012**, *8*, 209−213.

(2) Ohta, S.; Komagata, S.; Seki, J.; Saeki, T.; Morishita, S.; Asaoka, T. All-solid-state Lithium Ion Battery Using Garnet-type Oxide and Li_3BO_3 Solid Electrolytes Fabricated by Screen-printing. *J. Power Sources* **2013**, *238*, 53−56.

(3) Santhanagopalan, D.; Qian, D.; McGilvray, T.; Wang, Z.; Wang, F.; Camino, F.; Graetz, J.; Dudney, N.; Meng, Y. S. Interface Limited Lithium Transport in Solid-State Batteries. *J. Phys. Chem. Lett.* **2014**, *5*, 298−303.

(4) Kim, K. H.; Iriyama, Y.; Yamamoto, K.; Kumazaki, S.; Asaka, T.; Tanabe, K.; Fisher, C. A. J.; Hirayama, T.; Murugan, R.; Ogumi, Z. Characterization of the Interface Between $LiCoO_2$ and $Li_7La_3Zr_2O_{12}$ in an All-solid-state Rechargeable Lithium Battery. *J. Power Sources* **2011**, *196*, 764−767.

(5) Moriwake, H.; Kuwabara, A.; Fisher, C. A. J.; Huang, R.; Hitosugi, T.; Ikuhara, Y. H.; Oki, H.; Ikuhara, Y. First-Principles Calculations of Lithium-Ion Migration at a Coherent Grain Boundary in a Cathode Material, Li_xCoO_2. *Adv. Mater.* **2013**, *25*, 618−622.

(6) Wenzel, S.; Leichtweiss, T.; Krüger, D.; Sann, J.; Janek, J. Interphase Formation on Lithium Solid Electrolytes - an in Situ Approach to Study Interfacial Reactions by Photoelectron Spectroscopy. *Solid State Ionics* **2015**, *278*, 98−105.

(7) Iriyama, Y.; Inaba, M.; Abe, T.; Ogumi, Z. Preparation of C-axis Oriented Thin Films of $LiCoO_2$ by Pulsed Laser Deposition and Their Electrochemical Properties. *J. Power Sources* **2001**, *94*, 175−182.

(8) Yamada, I.; Iriyama, Y.; Abe, T.; Ogumi, Z. Lithium-ion Transfer on a Li_xCoO_2 Thin Film Electrode Prepared by Pulsed Laser Deposition - Effect of Orientation. *J. Power Sources* **2007**, *172*, 933−937.

(9) Xie, T.; Hasan, M. R.; Qiu, B.; Arinze, E. S.; Nguyen, N. V.; Motayed, A.; Thon, S. M.; Debnath, R. High-performing Visible-blind Photodetectors Based on SnO_2/*CuO* Nanoheterojunctions. *Appl. Phys. Lett.* **2015**, *107*, 241108.

(10) Debnath, R.; Xie, T.; Wen, B.; Li, W.; Ha, J. Y.; Sullivan, N. F.; Nguyen, N. V.; Motayed, A. A Solution-processed High-efficiency *p-NiO/n-ZnO* Heterojunction Photodetector. *RSC Adv.* **2015**, *5*, 14646−14652.

(11) Xie, T.; Sullivan, N.; Steffens, K.; Wen, B.; Liu, G.; Debnath, R.; Davydov, A.; Gomez, R.; Motayed, A. UV-assisted Room-temperature Chemiresistive NO_2 Sensor Based on TiO_2 Thin Film. *J. Alloys Compd.* **2015**, *653*, 255−259.

(12) Huang, R.; Hitosugi, T.; Fisher, C. A. J.; Ikuhara, Y. H.; Moriwake, H.; Oki, H.; Ikuhara, Y. Phase Transitions in $LiCoO_2$ Thin Films Prepared by Pulsed Laser Deposition. *Mater. Chem. Phys.* **2012**, *133*, 1101−1107.

(13) D'Hondt, H.; Hadermann, J.; Abakumov, A.; Kalyuzhnaya, A.; Rozova, M.; Tsirlin, A.; Nath, R.; Tan, H.; Verbeeck, J.; Antipov, E.; Van Tendeloo, G. Synthesis, Crystal Structure and Magnetic Properties of the $Sr_2Al_{0.78}Mn_{1.22}O_{5.2}$ Anion-deficient Layered Perovskite. *J. Solid State Chem.* **2009**, *182*, 356−363.

(14) Samal, D.; Tan, H.; Molegraaf, H.; Kuiper, B.; Siemons, W.; Bals, S.; Verbeeck, J.; Van Tendeloo, G.; Takamura, Y.; Arenholz, E.; Jenkins, C. A.; Rijnders, G.; Koster, G. Experimental Evidence for

DOI: 10.1021/acsami.5b12025
ACS Appl. Mater. Interfaces 2016, 8, 6727−6735

Oxygen Sublattice Control in Polar Infinite Layer $SrCuO_2$. *Phys. Rev. Lett.* **2013**, *111*, 096102.
(15) Tan, H.; Turner, S.; Yücelen, E.; Verbeeck, J.; Van Tendeloo, G. 2D Atomic Mapping of Oxidation States in Transition Metal Oxides by Scanning Transmission Electron Microscopy and Electron Energy-loss Spectroscopy. *Phys. Rev. Lett.* **2011**, *107*, 107602.
(16) Tan, H.; Tian, H.; Verbeeck, J.; Monico, L.; Janssens, K.; Van Tendeloo, G. Nanoscale Investigation of the Degradation Mechanism of a Historical Chrome Yellow Paint by Quantitative Electron Energy Loss spectroscopy Mapping of Chromium Species. *Angew. Chem., Int. Ed.* **2013**, *52*, 11360−11363.
(17) Tan, H.; Zhu, Y.; Dwyer, C.; Xin, H. L. Energy-loss- and Thickness-dependent Contrast in Atomic-scale Electron Energy-loss Spectroscopy. *Phys. Rev. B: Condens. Matter Mater. Phys.* **2014**, *90*, 214305.
(18) Kikkawa, J.; Terada, S.; Gunji, A.; Nagai, T.; Kurashima, K.; Kimoto, K. Chemical States of overcharged $LiCoO_2$ Particle Surfaces and Interiors Observed Using Electron Energy-Loss Spectroscopy. *J. Phys. Chem. C* **2015**, *119*, 15823−15830.
(19) Reimers, J. N.; Dahn, J. R. Electrochemical and in Situ X-Ray Diffraction Studies of Lithium Intercalation in Li_xCoO_2. *J. Electrochem. Soc.* **1992**, *139*, 2091−2097.
(20) Gabrisch, H.; Yazami, R.; Fultz, B. Hexagonal to Cubic Spinel Transformation in Lithiated Cobalt Oxide - TEM Investigation. *J. Electrochem. Soc.* **2004**, *151*, A891−A897.
(21) Wang, H.; Jang, Y.-I.; Huang, B.; Sadoway, D. R.; Chiang, Y.-M. TEM Study of Electrochemical Cycling Induced Damage and Disorder in $LiCoO_2$ Cathodes for Rechargeable Lithium Batteries. *J. Electrochem. Soc.* **1999**, *146*, 473−480.
(22) Shiraki, S.; Oki, H.; Takagi, Y.; Suzuki, T.; Kumatani, A.; Shimizu, R.; Haruta, M.; Ohsawa, T.; Sato, Y.; Ikuhara, Y.; Hitosugi, T. Fabrication of All-solid-state Battery Using Epitaxial $LiCoO_2$ Thin Films. *J. Power Sources* **2014**, *267*, 881−887.
(23) Tang, S.; Lu, L.; Lai, M. Characterization of a $LiCoO_2$ Thin Film Cathode Grown by Pulsed Laser Deposition. *Philos. Mag.* **2005**, *85*, 2831−2842.
(24) Takeuchi, S.; Tan, H.; Bharathi, K. K.; Stafford, G. R.; Shin, J.; Yasui, S.; Takeuchi, I.; Bendersky, L. A. Epitaxial $LiCoO_2$ Films as a Model System for Fundamental Electrochemical Studies of Positive Electrodes. *ACS Appl. Mater. Interfaces* **2015**, *7*, 7901−7911.
(25) Aurbach, D.; Markovsky, B.; Salitra, G.; Markevich, E.; Talyossef, Y.; Koltypin, M.; Nazar, L.; Ellis, B.; Kovacheva, D. Review on Electrode-electrolyte Solution Interactions, Related to Cathode Materials for Li-ion Batteries. *J. Power Sources* **2007**, *165*, 491−499.
(26) Gnanaraj, J.; Zinigrad, E.; Levi, M.; Aurbach, D.; Schmidt, M. A Comparison Among $LiPF_6$, $LiPF_3(CF_2CF_3)_3$ (LiFAP), and $LiN(SO_2CF_2CF_3)_2$ (LiBETI) Solutions: Electrochemical and Thermal Studies. *J. Power Sources* **2003**, *119−121*, 799−804.
(27) Tebbe, J. L.; Holder, A. M.; Musgrave, C. B. Mechanisms of $LiCoO_2$ Cathode Degradation by Reaction with HF and Protection by Thin Oxide Coatings. *ACS Appl. Mater. Interfaces* **2015**, *7*, 24265−24278.
(28) Matsui, M.; Dokko, K.; Kanamura, K. Dynamic Behavior of Surface Film on $LiCoO_2$ Thin Film Electrode. *J. Power Sources* **2008**, *177*, 184−193.
(29) Yazami, R.; Ozawa, Y.; Gabrisch, H.; Fultz, B. Mechanism of Electrochemical Performance Decay in $LiCoO_2$ Aged at High Voltage. *Electrochim. Acta* **2004**, *50*, 385−390.
(30) Goodenough, J. B.; Wakihara, M.; Li, G.; Ikuta, H.; Whittingham, M. S.; Yamaki, J.-I.; Winter, M.; Besenhard, J. O.; Nishi, Y.; Scrosati, B. *Lithium Ion Batteries: Fundamentals and Performance*; Wiley, 2007.
(31) Ohzuku, T.; Ueda, A. Solid-State Redox Reactions of $LiCoO_2$ (R-3m) for 4 V Secondary Lithium Cells. *J. Electrochem. Soc.* **1994**, *141*, 2972−2977.
(32) Kramer, D.; Ceder, G. Tailoring the Morphology of Li_xCoO_2: a First Principles Study. *Chem. Mater.* **2009**, *21*, 3799−3809.
(33) Egoavil, R.; Tan, H.; Verbeeck, J.; Bals, S.; Smith, B.; Kuiper, B.; Rijnders, G.; Koster, G.; Van Tendeloo, G. Atomic Scale Investigation of a $PbTiO_3/SrRuO_3/DyScO_3$ Heterostructure. *Appl. Phys. Lett.* **2013**, *102*, 223106.
(34) Tan, H.; Egoavil, R.; Béché, A.; Martinez, G. T.; Van Aert, S.; Verbeeck, J.; Van Tendeloo, G.; Rotella, H.; Boullay, P.; Pautrat, A.; Prellier, W. Mapping Electronic Reconstruction at the Metal-insulator Interface in $LaVO_3/SrVO_3$ Heterostructures. *Phys. Rev. B: Condens. Matter Mater. Phys.* **2013**, *88*, 155123.
(35) Bouwman, P.; Boukamp, B.; Bouwmeester, H.; Notten, P. Structure-related Intercalation Behaviour of $LiCoO_2$ Films. *Solid State Ionics* **2002**, *152-153*, 181−188.
(36) Balke, N.; Jesse, S.; Morozovska, A. N.; Eliseev, E.; Chung, D. W.; Kim, Y.; Adamczyk, L.; Garcia, R. E.; Dudney, N.; Kalinin, S. V. Nanoscale Mapping of Ion Diffusion in a Lithium-ion Battery Cathode. *Nat. Nanotechnol.* **2010**, *5*, 749−754.
(37) Gummow, R.; Liles, D.; Thackeray, M. Spinel Versus Layered Structures for Lithium Cobalt Oxide Synthesised at 400°C. *Mater. Res. Bull.* **1993**, *28*, 235−246.
(38) Gummow, R.; Liles, D.; Thackeray, M.; David, W. A Reinvestigation of the Structures of Lithium-cobalt-oxides with Neutron-diffraction Data. *Mater. Res. Bull.* **1993**, *28*, 1177−1184.
(39) Rossen, E.; Reimers, J.; Dahn, J. Synthesis and Electrochemistry of Spinel LT-$LiCoO_2$. *Solid State Ionics* **1993**, *62*, 53−60.
(40) Carroll, K. J.; Qian, D.; Fell, C.; Calvin, S.; Veith, G. M.; Chi, M.; Baggetto, L.; Meng, Y. S. Probing the Electrode/electrolyte Interface in the Lithium Excess Layered Oxide $Li_{1.2}Ni_{0.2}Mn_{0.6}O_2$. *Phys. Chem. Chem. Phys.* **2013**, *15*, 11128−11138.
(41) Qian, D.; Ma, C.; More, K. L.; Meng, Y. S.; Chi, M. Advanced Analytical Electron Microscopy For Lithium-ion Batteries. *NPG Asia Mater.* **2015**, *7*, e193.
(42) Arai, H.; Hayashi, M. Secondary Batteries-Lithium Rechargeable Systems-Lithium-ion | Positive Electrode: Lithium Cobalt Oxide. In *Encyclopedia of Electrochemical Power Sources*; Garche, J., Ed.; Elsevier: Amsterdam, 2009; pp 258−263.
(43) Takamatsu, D.; Koyama, Y.; Orikasa, Y.; Mori, S.; Nakatsutsumi, T.; Hirano, T.; Tanida, H.; Arai, H.; Uchimoto, Y.; Ogumi, Z. First in Situ Observation of the Li_xCoO_2 Electrode/Electrolyte Interface by Total-Reflection X-ray Absorption Spectroscopy. *Angew. Chem., Int. Ed.* **2012**, *51*, 11597−11601.
(44) Tan, H.; Verbeeck, J.; Abakumov, A.; Van Tendeloo, G. Oxidation State and Chemical Shift Investigation in Transition Metal Oxides by EELS. *Ultramicroscopy* **2012**, *116*, 24−33.
(45) Qian, D.; Xu, B.; Chi, M.; Meng, Y. S. Uncovering the Roles of Oxygen Vacancies in Cation Migration in Lithium Excess Layered Oxides. *Phys. Chem. Chem. Phys.* **2014**, *16*, 14665−14668.
(46) Egerton, R.; Li, P.; Malac, M. Radiation Damage in the TEM and SEM. *Micron* **2004**, *35*, 399−409.

DOI: 10.1021/acsami.5b12025
ACS Appl. Mater. Interfaces 2016, 8, 6727−6735